

A study of uranium-based multilayers: I. Fabrication and structural characterisation

R Springell^{1,2}, S W Zochowski¹, R C C Ward³, M R Wells³,
S D Brown^{2,4}, L Bouchenoire^{2,4}, F Wilhelm², S Langridge⁵,
W G Stirling^{2,4} and G H Lander⁶

¹Department of Physics and Astronomy, University College London, London WC1E 6BT, UK

²European Synchrotron Radiation Facility, BP220, F-38043 Grenoble Cedex 09, France

³Clarendon Laboratory, University of Oxford, Oxford OX1 3PU, UK

⁴Department of Physics, University of Liverpool, Liverpool L69 7ZE, UK

⁵ISIS, Rutherford Appleton Laboratory, Chilton, Oxfordshire OX11 0QX, UK

⁶European Commission, JRC, Institute for Transuranium Elements, Postfach 2340, Karlsruhe, D-76125, Germany

E-mail: ross.springell@esrf.fr

Abstract.

This paper addresses the structural characterisation of a series of U/Fe, U/Co and U/Gd multilayers. X-ray reflectivity has been employed to investigate the layer thickness and roughness parameters along the growth direction and high-angle diffraction measurements have been used to determine the crystal structure and orientation of the layers. For the case of uranium/transition metal systems, the interfaces are diffuse ($\sim 17\text{\AA}$) and the transition metals are present in a polycrystalline form of their common bulk phases with a preferred orientation along the closest packed planes; Fe, bcc (110) and Co, hcp (001), respectively. The uranium is present in a poorly crystalline orthorhombic, α -U state. In contrast, the U/Gd multilayers have sharp interfaces with negligible intermixing of atomic species, and have a roughness, which is strongly dependent on the gadolinium layer thickness. Diffraction spectra indicate a high degree of crystallinity in both U and Gd layers with intensities consistent with the growth of a novel hcp U phase, stabilised by the hcp gadolinium layers.

PACS numbers: 61.10.Kw, 61.10.Nz, 68.35.Ct, 68.55.Jk, 68.65.Ac

1. Introduction

The properties of a material can differ greatly from the bulk when reduced in size into the nanometre regime. The fabrication of multilayers results in the juxtaposition of different elements in systems where the interfacial regions comprise a substantial part of the whole sample, producing interesting electronic and magnetic effects. Varying the structural composition of the different elements can be used to manipulate the electronic and magnetic behaviour of the respective constituents [1]. The use of the actinide element uranium in such systems can be used to investigate effects arising from the unpaired $5f$ electrons, which exhibit strong hybridisation with other electronic states in uranium compounds [2]. This tendency for $5f$ hybridisation could lead to exotic properties in multilayers containing uranium.

The polarisation of uranium was reported in a study of the UAs/Co multilayer system [3, 4], where the proximity of the amorphous ferromagnetic UAs compound to the transition metal (TM) ferromagnet, Co, resulted in a large magneto-optical Kerr effect from the uranium [5]. The first reports of multilayers including uranium in its elemental form discuss the proximity effects of the transition metals Co [6] and Fe [7]. Our group has carried out a series of experiments on U/Fe multilayers [7, 8]. These papers discuss the fabrication and characterisation of a series of samples, using a combination of X-ray reflectivity (XRR), X-ray diffraction (XRD), Mössbauer spectroscopy, bulk magnetisation and polarised neutron reflectivity (PNR) techniques. Since these studies, modifications to the sputtering apparatus at the Clarendon laboratory, Oxford, have improved the control of the sputtering rates and the inclusion of a third sputter-gun has allowed the growth of buffer and capping layers to seed crystalline assembly of the bilayers and prevent oxidation of the multilayer stack. Recent measurements of the X-ray magnetic circular dichroism (XMCD) at the U M-edges have probed the electronic behaviour of the U $5f$ states in U/Fe multilayers [9] and confirmed earlier X-ray resonant magnetic reflectivity (XRMR) measurements [10], which demonstrate that a polarisation of the uranium $5f$ electrons occurs in the U/Fe multilayers as a result of the hybridisation of (U) $5f$ - $3d$ (Fe) electrons.

In the present articles (I and II), we report on a new series of U/Fe multilayers and extend our study to the transition-metal U/Co system. In addition, the fabrication and characterisation of a series of U/Gd multilayers is also described. In order to understand the growth mechanisms and structural properties of this range of systems it is helpful to recall the sizes of the respective atoms. The atomic volumes of Fe and Co are $\sim 12\text{\AA}^3$, whereas that of U is $\sim 21\text{\AA}^3$, assuming the latter to be in the room temperature, ambient form of the alpha phase, which has an orthorhombic crystal structure. The resulting mismatch in one dimension is $\sim 20\%$ and would result in a considerable compressive strain on the uranium. In contrast, the atomic volume of Gd is $\sim 33\text{\AA}^3$, giving a length mismatch of $\sim 14\%$ and a strain that is clearly in the opposite sense to that found when using $3d$ transition metal elements. These strains could result in significantly different structural and magnetic properties between the U/TM and U/Gd multilayers.

2. Fabrication

Multilayers were fabricated using a three-gun, dc magnetron sputtering assembly in a loadlocked growth chamber operating at UHV base pressure (5×10^{-10} mbar). Substrates were single-crystal sapphire plates, which were epi-polished parallel to the

(11 $\bar{2}$ 0) plane. A 50Å thick niobium buffer layer was used to seed crystalline growth of the bilayers. Nb has a body centred cubic (bcc) crystal structure and is expected to exhibit [110] preferred orientation on sapphire (11 $\bar{2}$ 0) when deposited at ambient temperature (it is fully epitaxial at elevated temperature). A similar Nb layer was used as a capping layer to prevent atmospheric attack of the multilayer after growth. A study of epitaxial (110) Nb films on sapphire has found that a stable layer of Nb₂O₅ ~ 20Å thick is formed, which provides effective long-term passivation [11].

Sputtering was carried out in a (flowing) argon pressure of 5×10^{-3} mbar, and a growth rate ~ 1Ås⁻¹ was employed for each element. Precise deposition rates were determined from measurement of calibration samples, by comparison of experimental and calculated X-ray reflectivity profiles. The majority of samples were grown at ambient temperature, although a substrate heater was available to investigate the effects of elevated temperature on selected samples.

3. Structural Characterisation

Series of U/Fe, U/Co and U/Gd samples were made in order to study the structural properties systematically as a function of the layer thicknesses of the respective elements, and to contrast and compare trends between the systems. In this paper the composition of the multilayers is represented as [A_X/B_Y]_Z, where A and B represent the elements comprising the bilayer system of interest, X and Y are the respective layer thicknesses (Å) as determined by X-ray reflectivity and Z is the number of bilayer repeats. In this case, element A is uranium and element B represents the ferromagnet, iron, cobalt or gadolinium. The samples were grown with layer thicknesses in the ranges $5 < t_U(\text{Å}) < 90$ and $10 < t_B(\text{Å}) < 80$. The X-ray reflectivity technique was employed to investigate the composition of the multilayers, in terms of the layer thickness and interface roughness values. High-angle X-ray diffraction measurements were used to investigate the crystal structures of the respective elements within the layers.

3.1. X-ray reflectivity

3.1.1. Experimental method X-ray reflectivity scans were carried out on a Philips diffractometer at the Clarendon Laboratory, Oxford. This diffractometer was optimised for low-angle diffraction measurements. A copper anode tube source provided Cu K α X-rays of wavelength 1.54Å, selected by a germanium monochromator and attenuated by a nickel foil to avoid detector saturation and to reduce Cu K β background. The scans were taken in a specular geometry with the scattering vector normal to the sample surface.

The data were fitted to simulations of the reflected intensity, based on a matrix method of interferometry that reduces to Parratt's recursive method [12]. The interface regions were modeled by a method proposed by Névoit and Croce [13], which was later adapted by others [14, 15, 16], which treats the layer roughnesses as a variation of the index of refraction. The simulations and fitting routines are part of the xPOLLY programme [17]. The reflectivity is calculated by a set of input parameters, including the anomalous scattering factors of the respective materials at the energy of the incident photons, the density (atoms/Å³), the layer thickness (Å) and the rms roughness (Å). All of these values can be varied, although in practice the scattering factors were kept constant and the structural parameters varied. The

initial structural models consist of a substrate, Nb buffer layer, repeated bilayer and an oxidised capping layer. Complexity can then be introduced by stratifying the bilayer to account for regions of reduced density at the interfaces, where strain, caused by lattice mismatches between relevant species, can produce defects affecting the crystal structure of the layers.

This technique provides an excellent measure of the bilayer thickness, but is limited in its sensitivity to the relative thicknesses of individual layers. Good fits to the data could be produced by simulations that varied in individual layer thickness by several angstroms. For this reason, the reflectivity was not considered in isolation, but consistency was maintained by consideration of the growth parameters and results from XRD, PNR and SQUID magnetometry measurements [18].

3.1.2. Results The results are presented for the specular reflectivity of U/Fe, U/Co and U/Gd systems respectively. The normalised reflected intensity is plotted against the wave-vector momentum transfer, Q (\AA^{-1}), normal to the sample surface, where 2θ is the scattering angle, $Q = 2k \sin \theta$ and the wavevector $k = \frac{2\pi}{\lambda}$. This scattering geometry probes the reflected intensity as a function of depth, where the X-rays are sensitive to the electron density profile.

Figure 1 shows example X-ray reflectivity spectra for U/Fe ((a) and (b)) and U/Co samples ((c) and (d)). The work of Beesley et al. [7] [8], based on conclusions made from Mössbauer spectroscopy measurements, stratified the iron layers into three components: a highly textured (110) bcc crystalline component with a magnetic moment value close to that in bulk Fe, a crystalline component with a reduced moment, and a region of amorphous, non-magnetic iron ($\sim 12\text{\AA}$) located at the interfaces. Further analysis of Mössbauer data and a consideration of the mechanism for the existence of non-magnetic Fe has led to a modified view of the iron layer structure. The non-magnetic iron component detected by Mössbauer spectroscopy indicates that the Fe atoms are in an environment that leads to equally populated spin-up and spin-down bands. This situation is most likely to occur in an alloy, formed by interdiffusion at the U/Fe interfaces. We now believe that the Fe layer is best described thus: $\text{UF}_{\text{e alloy}}|\text{Fe}_{\text{amorphous}}|\text{Fe}_{\text{bcc}}|\text{FeU}_{\text{alloy}}$. In reality, distinct boundaries will not exist between these respective components.

The total bilayer repeat distance can be determined with a precision of 0.1\AA , but the individual layer thicknesses could not be so well defined. However, restrictions were also fixed on these values based on the sputtering times and known calibrations. The roughness values alter the Bragg peak intensities and increases greater than $\sim 1\text{\AA}$ in the rms roughness per layer can result in major reductions in the reflected intensity. However, it is not possible to distinguish between interdiffusion and roughness at the interface since they produce equivalent effects in the specular reflected intensity. More information on the nature of the interfacial structure can be obtained by a combination of high-angle X-ray diffraction and X-ray reflectivity measurements.

The U/Fe samples analyzed previous to this work using X-ray reflectivity [7] were grown on glass substrates and did not include either a buffer or a capping layer to prevent oxidation. The use of an Nb capping layer reduces the complicated oxidation profile through the multilayer stack to a Nb/Nb₂O₅ surface layer. This gives a more simpler for the calculation of the reflected intensity and one which includes a similar surface contribution for all of the samples. For samples of similar thickness the single crystal, optically flat, sapphire substrates have reduced the respective roughness of

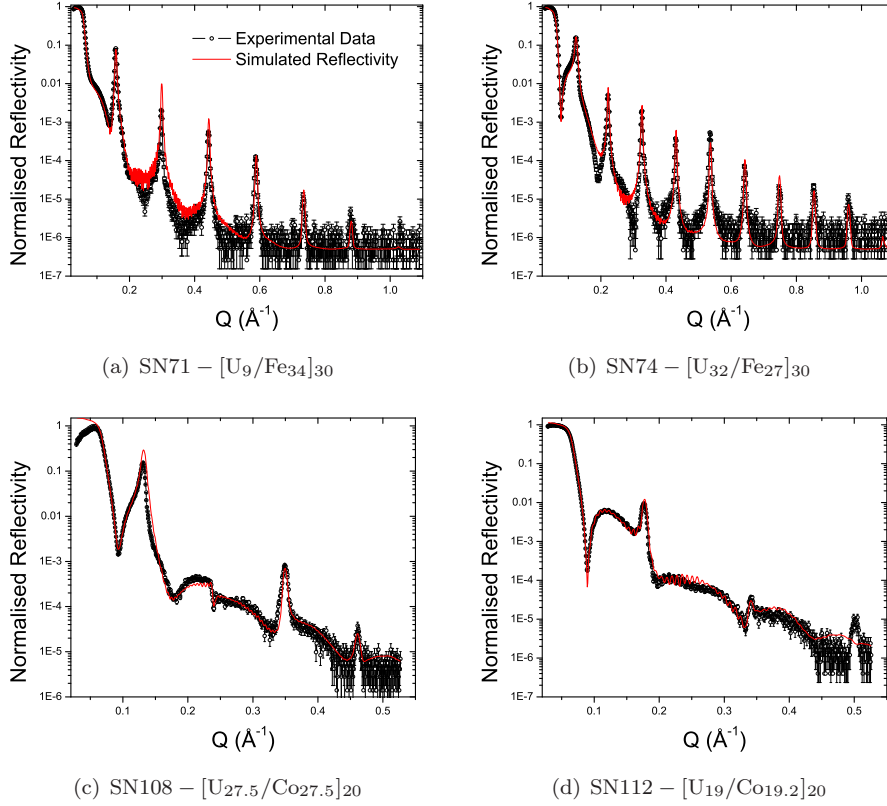


Figure 1. U/Fe and U/Co X-ray reflectivity spectra taken at room temperature, using a Cu $K\alpha$ X-ray source. Calculated reflectivity curves (shown in red) were fitted to the data using the xPOLLY programme. Layer thicknesses are as fitted; we note that the precision is of order 1\AA (see text).

the individual layers.

The reflectivity results for the U/Co samples were fitted by separating the cobalt layers into two components; one reduced density ($> 90\%$ of the bulk value) component of $\sim 15\text{\AA}$ thickness and the remainder of the bulk Co density, $\rho_{\text{Co}} = 9 \times 10^{28}\text{m}^{-3}$. This structural profile was determined from the polarised neutron reflectivity and bulk magnetisation measurements to be discussed in paper II [18] of this series. It was not possible to identify a U-Co alloy region at the interface as indicated by Mössbauer measurements on U/Fe samples, although it is likely to be present due to the similar atomic sizes of Fe and Co resulting in similar interfacial strains. The majority of the features observed in the reflected intensity have been reproduced in the simulations, including the extinction of even order Bragg peaks in the case of samples SN108 and SN112 in figure 1 (c) and (d), where the thicknesses t_{U} and t_{Co} are almost equal.

Figure 2 shows observed reflectivity spectra for a range of U/Gd multilayers. Panels (a) and (b) have similar bilayer repeat thicknesses, but vary in composition between thick Gd layers and thick U layers respectively. The difference in the spectra is striking; for large values of t_{Gd} (a) the reflected intensity decreases rapidly as a function of Q (\AA^{-1}), compared with the observation of well-defined Bragg peaks over

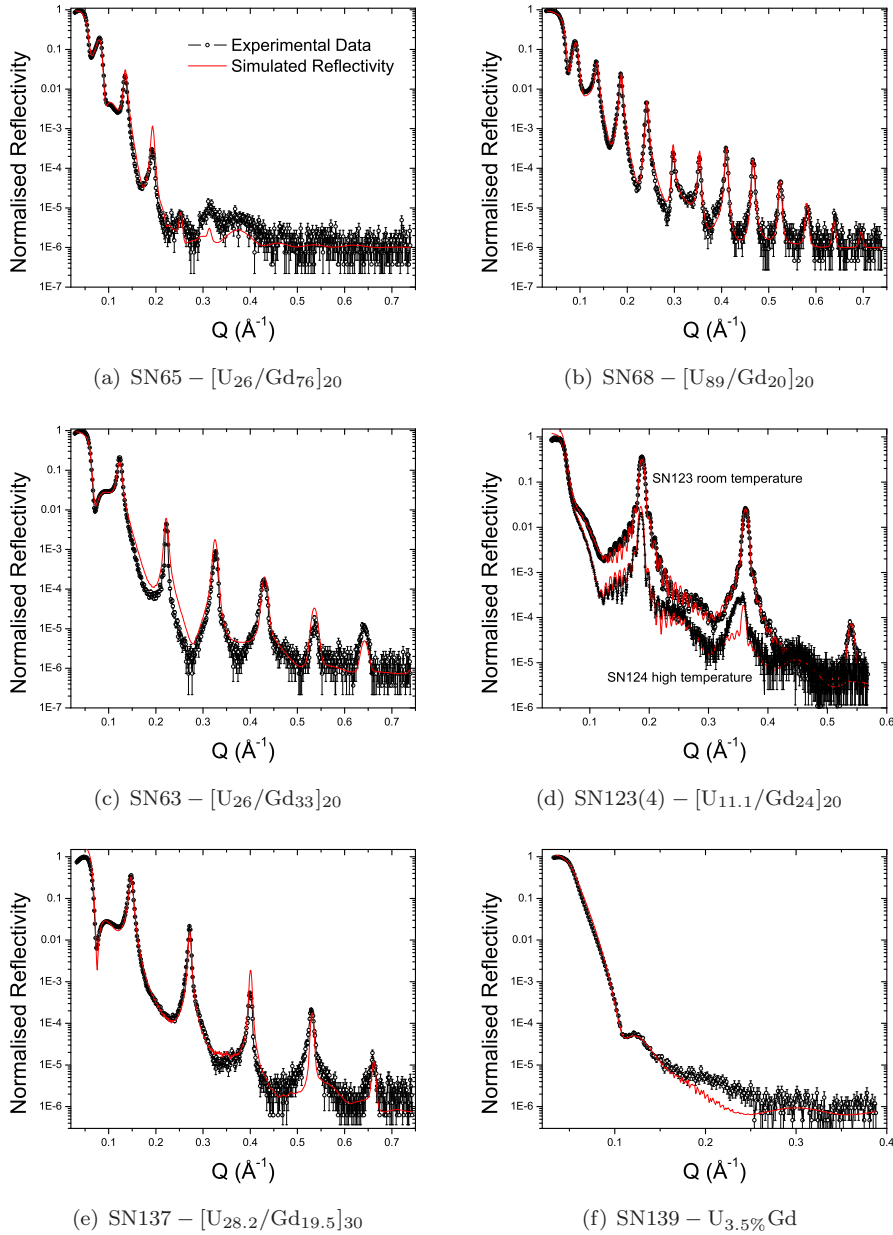


Figure 2. U/Gd X-ray reflectivity spectra taken at room temperature, using a Cu K α X-ray source. Calculated reflectivity curves (shown in red) were fitted to the data using the xPOLLY programme [17]. Note that the sample SN139 shown in panel (f) is not a multilayer, but a sputtered alloy of $\sim 3.5\%$ U in Gd.

a wide Q-range in the reflectivity spectra of samples with thick U layers, e.g. (b). The graphs (a), (c) and (e) show the reflectivity curves for samples of decreasing Gd layer thickness for almost constant values of t_U and indicate a reduction in the bilayer roughness for thin Gd layers. Figure 2 (d) compares the observed reflectivity for two like samples grown at different temperatures and (f) contrasts the reflectivity spectrum observed for a U-Gd alloy sample with those of U/Gd multilayers.

3.1.3. Discussion The general good quality of multilayer samples in all cases is supported by the form of the measured X-ray reflectivity profiles. The relative growth properties of U/Fe samples grown on sapphire substrates with niobium buffer and capping layers, can be compared to those grown previously on glass with no buffer or capping layers [7], by comparing relative thickness and roughness parameters. The roughness of layers in the latter, although $\sim 1 - 2\text{\AA}$ larger for samples of similar layer thickness, are of approximately the same magnitude, indicating that the bilayer growth mechanisms are the same in both cases and that the majority of the roughness stems from the relative lattice mismatch and crystalline nature of the respective species. The slightly reduced roughness in the new samples can be understood as an effect of the smooth substrate surface and low roughness value of the niobium buffer layer.

Both U/Fe and U/Co samples were modeled by separating the ferromagnetic layers into two components; one with a reduced density (10% less than the bulk value), $\sim 15\text{\AA}$ thick, and the remainder of the layer with the bulk density. This model is supported by results obtained in PNR, Mossbauer and SQUID magnetometry [7] [8] measurements, discussed in paper II [18], and can be understood by considering the growth of layers with a large mismatch in lattice spacings, $\sim 20\%$. The large strains and diffusion of the smaller transition metal atoms into the uranium layers produce an alloyed region at the interfaces. Growth of the ferromagnetic layers onto these alloys produces an initial amorphous, noncrystalline form, but as the layer thickness is increased the layer tends towards a bulk crystalline state.

All uranium/gadolinium samples were modeled with a simple bilayer structure, since magnetisation measurements [18] have not revealed the presence of any substantial 'dead' layer, requiring a stratified density gadolinium layer. X-ray diffraction measurements (described in section 3.2) indicate a much lower lattice mismatch between U and Gd layers than that observed in the transition metal systems, which could lead to a more coherent layer by layer growth and therefore not require such a complex description of the gadolinium layer structure. As shown in figure 2 and table 1, for thick uranium layers a large number of Bragg peaks were observed over a wide Q range, characterised by a low rms roughness of $\sim 4\text{\AA}$ per layer. For an equivalent bilayer thickness, but with thick gadolinium layers, the roughness was larger, possibly caused by a more columnar crystal growth, resulting in a step-like roughness profile. The large difference between the X-ray reflectivity in these two cases was not apparent for similar situations in the U/Fe and U/Co systems.

Tables 1 (a) and (b) show the rms roughness values for a selection of U/Gd samples; a set with constant t_U and increasing t_{Gd} and a series with constant t_{Gd} and varying t_U . Average roughness values are given in \AA for the uranium (σ_U) and gadolinium (σ_{Gd}) layers, and σ_{av} represents an average roughness per bilayer. Similar to the determination of individual layer thicknesses from the simulation of the X-ray reflectivity spectra, the individual layer roughnesses were also difficult to distinguish precisely, although the intensities were very sensitive to σ_{av} . However, the vast majority of samples studied indicated larger roughness values for the gadolinium

Table 1. Roughness values per layer ($\text{\AA} \pm 10\%$) as a function of (a) gadolinium thickness and (b) uranium layer thickness.

(a)

Sample	Composition	σ_U	σ_{Gd}	σ_{av}
SN63	[U ₂₆ /Gd ₃₃] ₂₀	3.2	7.0	5.1
SN64	[U ₂₆ /Gd ₅₄] ₂₀	7.0	7.0	7.0
SN65	[U ₂₆ /Gd ₇₆] ₂₀	9.0	10.0	9.5

(b)

Sample	Composition	σ_U	σ_{Gd}	σ_{av}
SN66	[U ₃₉ /Gd ₂₀] ₂₀	3.0	5.0	4.0
SN67	[U _{63.5} /Gd ₂₀] ₂₀	3.2	5.5	4.4
SN68	[U ₈₉ /Gd ₂₀] ₂₀	2.9	5.0	4.0

layers than for the uranium. Table 1 (a) shows a near linear relationship between t_{Gd} and σ_{av} , where thicker Gd layers result in large rms roughness values. In contrast, table 1 (b) shows a practically constant σ_{av} for a range of U layer thicknesses.

3.2. X-ray Diffraction

The previous section has dealt with the use of X-rays to probe the physical composition of the multilayers on length scales $\sim 10 \rightarrow 1000\text{\AA}$, perpendicular to the plane of the sample. It is also important, however, to be able to determine the crystal structure and orientation of the respective layers and various properties of the crystallites that have formed. A study of this type gives insight into the growth mechanisms and interfacial structure of the multilayer samples. X-ray diffraction is the most commonly used and readily available tool for the investigation of these properties.

Due to the likely lattice mismatch between the respective elements in the case of U/TM and U/Gd systems the samples considered here are likely to be composed mainly of polycrystalline layers with a preferred orientation and a range of crystallite sizes.

3.2.1. Results The results are presented for the X-ray diffraction in a $\theta - 2\theta$ geometry for U/Fe, U/Co and U/Gd systems, respectively. Summaries of the X-ray diffraction patterns for U/Fe and U/Co systems are presented in figures 3 (a) and (b), whereas figures 4 and 5 summarise the series of U/Gd samples. The diffracted intensity is plotted against the momentum transfer, Q (\AA^{-1}), for each series of samples in order to compare qualitatively structural variations of the properties across the series. The intensity is normalised to unity at the peak of the scattering from the sapphire substrate.

The upper panel of figure 3 shows a summary of the X-ray diffraction patterns taken for the U/Fe series of samples. The intense peak at 2.643\AA^{-1} is due to the epitaxial sapphire substrate and the satellite peaks that appear on the low angle side of the substrate peak are a consequence of the $\sim 50\text{\AA}$ thick niobium buffer layer. The

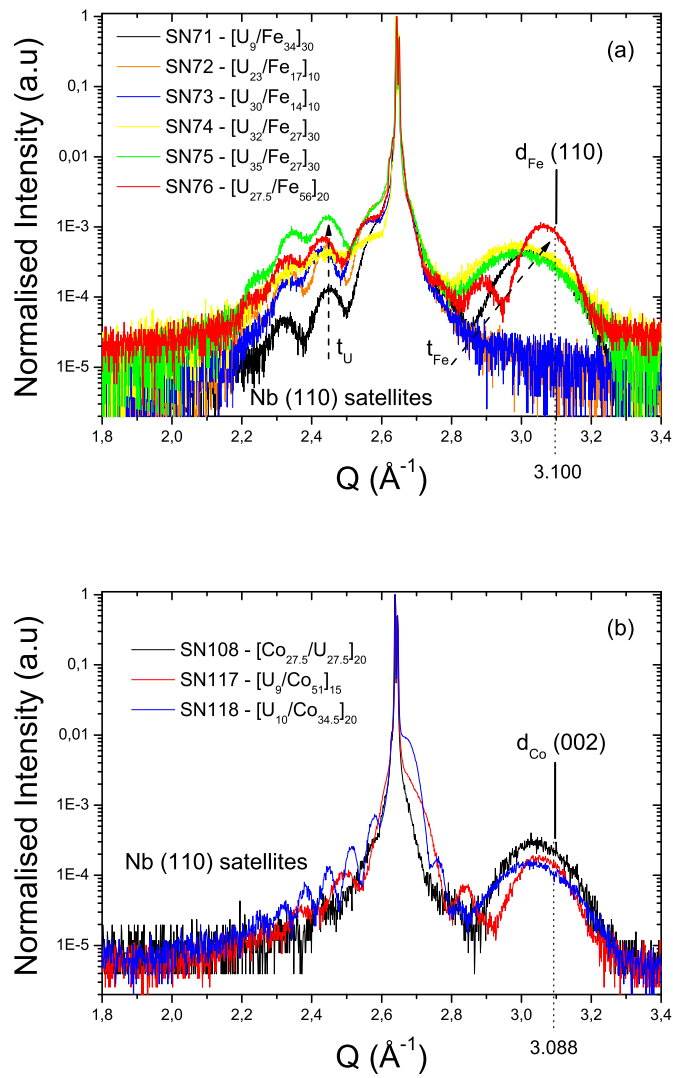


Figure 3. Comparison of the X-ray diffraction patterns close to the sapphire (11 $\bar{2}$ 0) peak, for selected U/Fe samples (upper panel) and selected U/Co samples (lower panel). The arrows in panel (a) indicate increasing U and Fe layer thicknesses. The d-spacings of Fe (110) and Co(002) are indicated.

α -uranium (110), (021) and (002) peaks were observed previously in diffraction spectra of U/Fe multilayers grown on glass [7] and were positioned at 2.448\AA^{-1} , 2.490\AA^{-1} and 2.537\AA^{-1} respectively for the Cu-K α wavelength. In our case, these peaks cannot be observed due to the presence of the Nb buffer diffraction peaks, whose intensity is a consequence of the crystalline quality of the niobium layer. However, it is possible to see an increase in the background intensity at the α -uranium peak positions, dependent on the thickness of the uranium layers.

The broad hump on the high-angle side of the substrate peak is close to the bulk bcc (110) iron position and there are no peaks at other allowed bcc Fe crystallographic directions, suggesting a preferred orientation in this growth direction. This confirms predictions considering only the likely growth in the direction of the most closely packed plane as discussed earlier. The lack of any intensity at all at iron layer thicknesses of $< 20\text{\AA}$ suggests that this represents a crystalline limit, below which the growth would be expected to be amorphous and consequently of reduced magnetisation. The positions of the iron peaks were used to deduce values for the average lattice spacing in the growth direction, d_{Fe} , and the mean crystallite size, D , was determined by measuring the width of the peaks and using the Scherrer equation. This states that as the diffracting volumes become smaller the peaks broaden, giving a finite $\Delta\theta$ width. The size of the diffracting particles, D , is given by $D = \frac{K\lambda}{\Delta\theta \cos\theta_B}$, where $K=0.9394$ and θ_B is the Bragg angle [19]. Values for d_{Fe} and D , determined by this method are given in table 2 for a selection of U/Fe samples.

Table 2. Lattice spacings (d_{Fe}) and particle sizes (D) of Fe layers for a selection of U/Fe samples, determined by an investigation of the diffraction peak positions and widths, using the Scherrer formula. For bulk bcc Fe $d_{(110)} = 2.027\text{\AA}$.

Sample Number	Composition	d_{Fe} ($\text{\AA} \pm 0.005$)	D ($\text{\AA} \pm 2$)
SN71	[U ₉ /Fe ₃₄] ₃₀	2.052	31.0
SN74	[U ₃₂ /Fe ₂₇] ₃₀	2.073	23.5
SN75	[U _{35.2} /Fe ₂₇] ₃₀	2.073	23.1
SN76	[U _{27.5} /Fe ₅₇] ₃₀	2.045	49.4

The average lattice spacings are larger than the bulk Fe value of $d = 2.027\text{\AA}$, indicating an overall lattice expansion. As the thickness of the iron layer is increased the lattice spacing approaches that of the bulk value for a bcc ([110] oriented) crystal. The particle size scales with Fe layer thickness, but is several \AA thinner than the Fe layers. This is consistent with the picture of a non-coherent growth between the α – U and Fe atoms; crystallites which do not extend across more than one layer due to the poor registry between Fe and U crystal planes and regions of alloy at the interfaces.

The lower panel of figure 3 shows a summary of the X-ray diffraction patterns taken for several U/Co samples. The changing period of the niobium satellites can be seen on the low-angle side of the sapphire substrate peak as the buffer thickness is changed; SN117 has $\sim 50\text{\AA}$ Nb and SN118, $\sim 100\text{\AA}$ Nb. It was not possible to see any effect of varying t_U on the observed diffracted intensity. The diffraction patterns for the U/Co series of samples are remarkably similar in character to those of the U/Fe system, since the position of the hcp (002) cobalt peak lies at almost exactly the same wavevector as that for bcc (110) iron. The nature of the broad hump on the high-angle side of the substrate peak is influenced by the thickness of the cobalt layers

and a similar relationship can be observed between t_{Co} and the diffracted intensity of the cobalt layers as was seen for the U/Fe series of samples.

The observed intensity of the cobalt hcp (002) peak, while no other peaks are observed at other allowed hcp Co crystallographic directions, indicates a preferred orientation in this growth direction, expected since it is the most closely packed plane within the hcp crystal structure. The average particle size, D , and the lattice spacing, d_{Co} , were determined, using the same method outlined for the U/Fe samples, and these are summarised in table 3.

Table 3. Lattice spacings and particle sizes of Co layers for a selection of U/Co samples, determined by an investigation of the diffraction peak positions and widths, using the Scherrer formula. For bulk hcp Co $d_{(002)} = 2.035\text{\AA}$.

Sample Number	Composition	d_{Co} ($\text{\AA} \pm 0.005$)	D ($\text{\AA} \pm 2$)
SN116	$[\text{U}_{19}/\text{Co}_{42.5}]_{20}$	2.064	28.3
SN117	$[\text{U}_9/\text{Co}_{51}]_{15}$	2.058	43.2
SN118	$[\text{U}_{10}/\text{Co}_{34.5}]_{20}$	2.075	31.7

Samples SN117 and SN118 described in figure 3 (lower panel) and table 3 were grown at an elevated substrate temperature of $\sim 450\text{K}$. These samples allow both a layer thickness dependent and a temperature dependent comparison to be made. For all U/Co samples, the particle sizes follow a similar trend to that observed for the U/Fe system, although the crystallite sizes are larger in proportion to the Co layer thicknesses for the samples grown at elevated temperature. As for the U/Fe samples, the lattice spacings are expanded compared to the bulk, but tend towards the bulk value as t_{Co} increases.

Figure 4 shows a summary of the X-ray diffraction patterns taken for a series of U/Gd samples. There are a number of striking differences in the form of the diffracted intensity between the U/TM metal and the U/Gd multilayers. The multilayer diffraction peaks occur on the low- Q side of the sapphire substrate peak and their intensity reaches values up to one tenth of the intensity of the substrate peak, more than two orders of magnitude larger than the intensity observed for the U/Fe and U/Co systems. This indicates a far greater degree of crystallinity for U/Gd than for U/TM samples. The diffraction satellites from the highly crystalline niobium buffer layers are not observable in most cases above the multilayer diffraction peaks, although a contribution from the niobium can be observed as a shoulder on the low angle side of the substrate peak. A gadolinium film (SN62) of $\sim 500\text{\AA}$ was grown to confirm the expected position of the diffraction peaks in the multilayer samples and diffraction data for this sample are shown as the dashed curve in figure 4.

The series of U/Gd multilayers of figure 4 was grown to investigate the relationship between t_{Gd} and t_{U} on the structural and magnetic properties of the U/Gd system. The accepted values for the lattice parameters of the hexagonal close-packed crystal structure of gadolinium are $a = 3.631\text{\AA}$ and $c = 5.777\text{\AA}$, giving a contraction from the hard sphere model for the c/a ratio (1.633) to 1.591. In these measurements we are sensitive only to length scales in the z -axis direction, perpendicular to the plane of the film, so our discussion will centre around the c -axis lattice parameter and the lattice spacings.

In the case of the single film of gadolinium the (002) peak is centred at a Q value

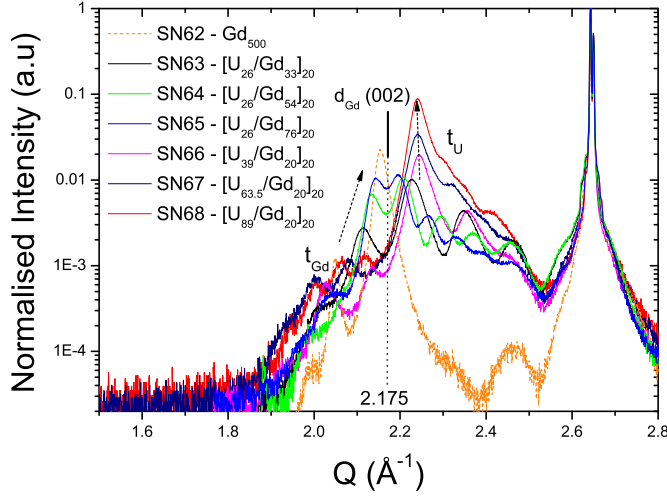


Figure 4. Comparison of the X-ray diffraction patterns close to the sapphire (11 $\bar{2}$ 0) peak, for a series of U/Gd samples. The dashed orange peak represents the diffraction from a 500Å thick sputtered Gd film, which results in a lattice spacing, d_{Gd} of 2.92Å. The position of the bulk values is also noted.

of 2.152\AA^{-1} , corresponding to a c-axis lattice parameter of 5.840\AA , an expansion from the bulk of about 1%. It is also possible to observe intensity from the niobium buffer at 2.450\AA^{-1} and a peak at 2.040\AA^{-1} , corresponding to the hcp (100) reflection that occurs in the bulk at 1.998\AA^{-1} . This shift to higher Q in the thin Gd film suggests a contraction of the lattice along the basal plane of $\sim 2\%$ towards a value of $a = 3.556\text{\AA}$ and a c/a ratio of 1.642.

Indicated by a dashed arrow on figure 4, as t_{Gd} increases there is a distinct increase in intensity of one of the component peaks in the diffraction patterns, close to the hcp (002) peak observed for the thin Gd film. This increase in intensity is accompanied by a shift in position from the low angle side of the (002) peak towards the thin film value, indicating a lattice expansion for thinner Gd layers.

As the uranium layer thickness, t_{U} , is varied there is a clearly visible increase in the intensity of one of the component peaks in the X-ray diffraction spectra, at 2.245\AA^{-1} . This peak does not relate to any of the known peak positions in the α -U phase, but could correspond to the (002) peak of an [001] preferred orientation hcp-U crystal structure. Recent theoretical and experimental evidence [20, 21] supports the existence of a stable hcp-U phase established in thin film structures, for an uranium film grown on a [110] oriented bcc, tungsten single crystal substrate. STM images [20] have described a hexagonal arrangement of atoms with a U-U distance of $a = 3.5 \pm 0.5\text{\AA}$, although a previous report by Molodtsov et al. [21] suggested a U-U distance of $3.2 \pm 0.5\text{\AA}$. A theoretical model [20], employing the local density approximation (LDA) supports the idea that an hcp-U crystal structure can be stabilised with a c/a axis ratio of 1.8, appreciably larger than the hard sphere, hcp model value of 1.633. The predicted values for c and a are 5.35\AA and 2.97\AA , respectively. However, it is accepted that there is a tendency for the LDA theory to over-compress the lattice and the actual values for the c and a axis parameters may be larger than these values.

Assuming the uranium stacks along the [001] axis, a reflection would be observed in the diffraction spectrum at $Q \sim 2.3\text{\AA}^{-1}$, which is close to the position of the diffraction peak attributed to the uranium in figure 4. Moreover, this peak position results in a lattice spacing along the c-axis only 5% larger than that expected for gadolinium, which could provide the mechanism for the growth and orientation of the exotic hcp (001) phase of uranium.

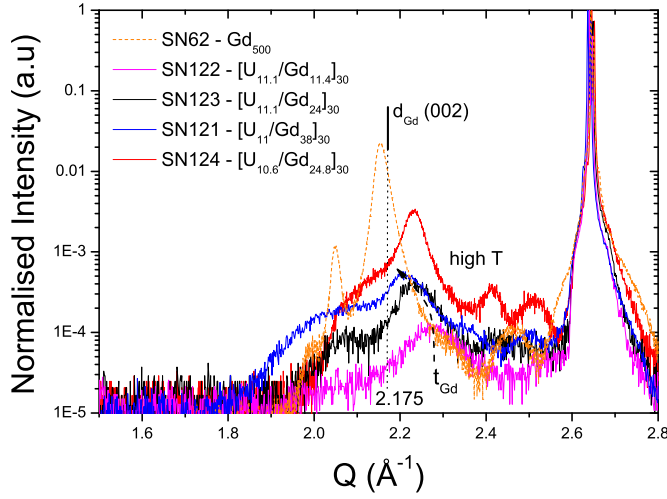


Figure 5. Comparison of the X-ray diffraction patterns close to the sapphire (11 $\bar{2}$ 0) peak, for a selection of U/Gd samples. The dashed peak represents the diffraction from a 500 \AA thick sputtered Gd film, which results in a lattice spacing, d_{Gd} of 2.92 \AA . The position of the bulk gadolinium lattice spacing is also noted.

Figure 5 shows a summary of the X-ray diffraction patterns taken for a series of U/Gd multilayers grown to investigate samples with thin layers, $< 20\text{\AA}$, and to observe the effect of increased substrate temperature on the crystalline structure. The thinnest of these films (SN122) had a bilayer thickness of just 22.5 \AA yet an appreciable diffracted intensity was still observable. It is clear that the crystalline limit for this multilayer system exists only for very thin layers. All of the samples shown in figure 5 consist of thin uranium layers of approximately 11 \AA . The prominent peak in these diffraction spectra occurs at the hcp-U peak position observed previously, which shifts to lower Q as the gadolinium layer thickness increases. This indicates that the uranium grows in a more crystalline manner than the gadolinium layers at low values of t_{U} and t_{Gd} respectively, and that as t_{Gd} increases the average U lattice spacing is increased, possibly as a consequence of the Gd crystallinity. Samples SN123 and SN124 share similar compositions, but were grown at room temperature and an elevated substrate temperature of 600K respectively. The diffracted intensity of the latter shares the same characteristics as that grown at room temperature, but is more than an order of magnitude greater, indicating a more crystalline assembly at elevated temperatures. Recalling the X-ray reflectivity from these two samples (see figure 2 (d)) along with the information taken from the high-angle diffraction measurements it is reasonable to infer that the relative amount of interdiffusion between the U and Gd species is small even at elevated growth temperatures. Remembering also the summary of the microstructural growth properties for sputtered films [22], as the

substrate temperature is increased the ratio T/T_m increases, where T_m is the melting point of the respective elements, suggestive of a more columnar crystal growth, which could be responsible for the large rms roughness needed to provide the rapid decay of intensity observed in the X-ray reflectivity spectrum for sample SN124.

3.2.2. Discussion The U/Fe series of samples considered within this study can be compared directly to results published previously [7, 8], to investigate the differences and similarities in the growth of the two sets of multilayers. Figure 6 (a) compares the lattice spacings, d_{Fe} , and figure 6 (b), the particle sizes taken from the structural characterisation results published by Beesley et al. [7] with those obtained more recently for the samples grown on sapphire substrates with niobium buffer and capping layers. The particle sizes of the two sets of samples follow the same trend, tending to increase with increasing Fe layer thickness. The lattice parameter, however, seems to follow a much steeper exponential trend towards the bulk value for large t_{Fe} in the case of samples grown on sapphire than for those grown on glass.

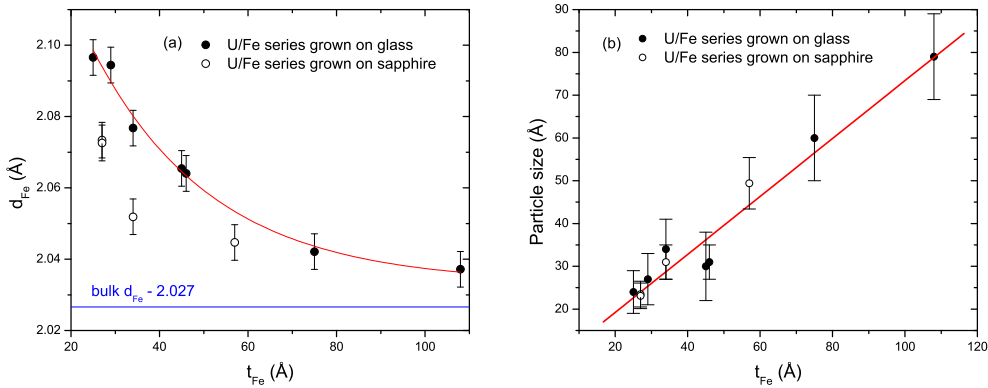


Figure 6. Comparison of (a) the iron lattice spacings, d_{Fe} , and (b) particle sizes for U/Fe samples grown on glass [7, 8] and those grown on sapphire (present work).

The U/Gd diffraction spectra are markedly different from those observed for the U/TM multilayers investigated thus far. The peaks attributed to the hcp Gd (002) and hcp U (002) crystalline phases exhibit a mismatch of $< 5\%$, resulting in the presence of satellite peaks either side of these primary ones. This observation is a direct consequence of a coherent growth between respective U and Gd layers, giving coherent scattering from crystalline planes in many layers.

Table 4 compares the bilayer thicknesses determined by both high- and low-angle X-ray diffraction methods for a series of U/Gd samples. For the samples with thick Gd layers, the values of the bilayer thickness determined by the separation of the high-angle diffraction satellites are consistently $\sim 8\text{\AA}$ lower than those indicated by X-ray reflectivity measurements, whereas for samples with thick U layers the values are only $\sim 2.5\text{\AA}$ lower. This result suggests that a small region of the bilayer is not crystalline (likely to be present at the interface), and that this noncrystalline component is larger in samples with thick Gd layers than in those with large t_U . This result is consistent with the variation in roughness in the X-ray reflectivity measurements.

Table 4. Comparison of the bilayer thicknesses for (a) samples with increasing t_{Gd} and (b) samples with increasing t_{U} , determined by both high (t_{Bdif}) and low angle (t_{Bref}) X-ray diffraction. \bar{x} represents the average separation of the high-angle diffraction satellites in \AA^{-1} .

(a)			
t_{Gd} ($\text{\AA} \pm 2$)	\bar{x} (\AA^{-1})	t_{Bdif} ($\text{\AA} \pm 2$)	t_{Bref} ($\text{\AA} \pm 2$)
33.0	0.122	51.5	59
54.0	0.087	72.2	80
76.0	0.067	93.8	102

(b)			
t_{U} ($\text{\AA} \pm 2$)	\bar{x} (\AA^{-1})	t_{Bdif} ($\text{\AA} \pm 2$)	t_{Bref} ($\text{\AA} \pm 2$)
39.0	0.110	57.1	59.0
63.5	0.078	80.6	83.5
89.0	0.059	106.5	109.0

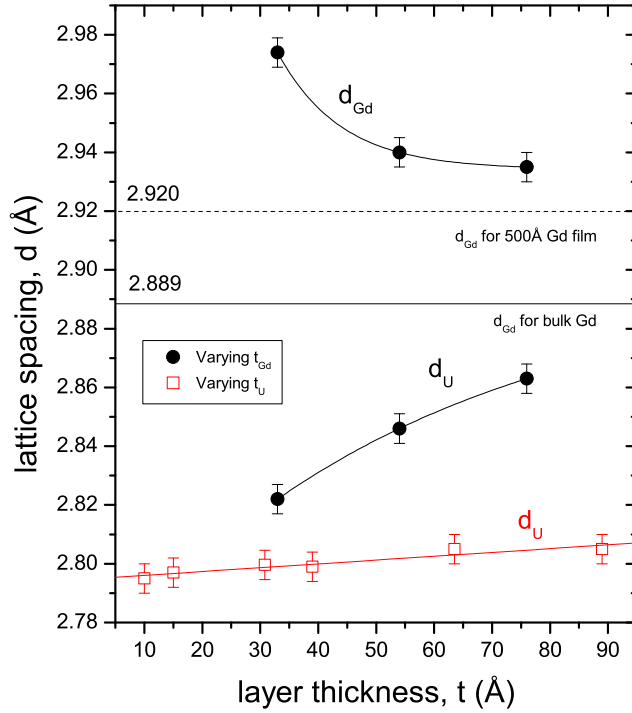


Figure 7. Variations in the lattice spacings of uranium and gadolinium as a function of t_{Gd} (full points) and t_{U} (open squares). Values for the bulk and thick Gd film gadolinium lattice parameter are labeled. Solid lines are guides for the eye.

When the layers grow coherently in a multilayer it is possible for variations in the layer thickness of one element to affect the strain profile of another, which will be reflected in the lattice spacing values. Figure 7 summarises the lattice spacing values as determined from the X-ray diffraction profiles for a number of U/Gd samples. The variation of both d_{Gd} and d_{U} are shown as a function of t_{Gd} , full points (black), the dependence of the uranium lattice parameter upon the U layer thickness is represented by the open squares (red). It was not possible to distinguish the gadolinium diffraction peak positions in the case of varying t_{U} , since the gadolinium layers were too thin to give an appreciable diffracted intensity.

As described earlier, the lattice parameter in a sputtered thin film of gadolinium (2.920\AA) is expanded compared to that of bulk Gd (2.899\AA); both of these values are clearly marked in figure 7. For multilayers containing thin gadolinium layers the Gd lattice is further expanded, but contracts towards the sputtered thin film value as the layers become thicker. There is very little observable change in the U lattice spacing, d_{U} , as t_{U} is varied. For the case of these samples the gadolinium layer thickness is constant at 20\AA . However, a slight expansion of the lattice is observable for thick U layers. An interesting result observed here is the dependence of d_{U} upon the gadolinium layer thickness, with $t_{\text{U}} \sim 26\text{\AA}$. A consideration of the lattice parameter sizes of the hcp (001) Gd and hcp (001) U phases, reveals a likely strain acting to expand the U lattice. The trend observed in figure 7 implies an increase in the strain acting on the U layers, as t_{Gd} is increased, which provides a mechanism for the observed increase in d_{U} .

4. Conclusions

The X-ray reflectivity spectra of all samples display well-defined Bragg peaks, which give accurate determinations of the bilayer thickness. The thicknesses of the individual layers are then obtained by maintaining consistency across a range of measurements. The inclusion of niobium buffer and capping layers has considerably reduced the complexity of the structural model required to simulate the reflectivity spectra of previous samples [7].

No significant improvement was observed in the crystalline growth of U/Fe samples on sapphire substrates with a Nb buffer layer when compared with those grown on glass [7]. The poor crystalline quality arises from the large mismatches in atomic sizes and lattice spacings at the U/Fe interfaces and chemical diffusion processes; this situation is replicated in the U/Co system. The similarities between the U/transition metal systems stem from the similar atomic volumes, resulting in no significant diffracted intensity observable from the U layers in these systems. The interdiffusion at the interfaces, causing an alloy region, observable as a nonmagnetic Fe component in earlier Mössbauer spectroscopy data [8] is likely to occur also in the U/Co system. The further determination of an amorphous (reduced moment) ferromagnetic component from this data explains the lack of diffracted intensity for U/Fe multilayers with $t_{\text{Fe}} < 20\text{\AA}$. The proposed structure for the ferromagnetic layers in U/transition metal systems is then: $\text{UT}_{\text{alloy}}|\text{T}_{\text{amorphous}}|\text{T}_{\text{crystalline}}|\text{TU}_{\text{alloy}}$, where T represents the transition metals iron and cobalt.

The situation in the case of the U/Gd system is considerably different. Although an atomic volume mismatch in one dimension of $\sim 14\%$ is still present between U and Gd, the strain is in the opposite sense to that present in U/Fe and U/Co multilayers. The outcome is the observation of an intense diffraction peak that does not correspond

to any known for $\alpha-U$, but at a position close to that reported for a novel hcp phase of uranium [20]. The lattice spacing, d_U , determined by this peak for thick U layers is about 2.80\AA and does not change significantly as the U layer thickness is varied (for constant t_{Gd} of 20\AA). This gives a c-axis lattice parameter for hcp uranium of 5.60\AA , somewhat larger than values put forward in the study of uranium grown on tungsten [20]. Assuming the same atomic volume of 20.5\AA^3 for hcp U as that for $\alpha-U$ and taking the c-axis parameter determined from X-ray diffraction measurements, the resulting a-axis value is 2.91\AA , giving a c/a ratio close to 1.9, much larger than that expected from a hard sphere model of the crystal structure. The lattice parameter of the a-axis also represents the U-U nearest neighbour distance in the hcp crystal structure, which in the $\alpha-U$ phase is 2.84\AA . A comparison of the local environments of U atoms in these two structures reveals a considerable change in the coordination and a lattice expansion of $\sim 2.5\%$. The observation of such intense diffraction spectra is then remarkable, considering the likely in-plane lattice spacings. We hope to verify these findings directly with further experiments. The mismatch, between the Gd ($a = 3.56\text{\AA}$ for the sputtered film) and hcp U ($a \sim 2.91\text{\AA}$) is $\sim 22\%$, yet growth along the common c-axis remains good. This result implies that considerable strains are present at the U/Gd interfaces, extending perhaps to a considerable distance into both layers.

The mismatch between the Gd hcp (001) and U hcp (001) lattice parameters along the c-axis is less than 5%, which explains the observation of satellite diffraction peaks, produced by coherent scattering from crystalline planes in many different layers. The bilayer thickness values determined from the separation of the satellite peaks were several ångström less than those determined by X-ray reflectivity, indicating a small interface region of noncrystalline material. A comparison of the U/Gd and the U/Co systems, suggests that such crystalline growth of the U layers in the U/Gd system is not simply due to the hexagonal packing arrangement of the gadolinium atoms, since the Co layers also adopt the hcp (002) crystal structure, but is due to the larger Gd atomic volume and possibly also to the different electronic configurations of the element.

X-ray reflectivity measurements of U/Gd multilayers revealed a strong dependence of the average roughness per bilayer upon the gadolinium layer thickness, suggesting a step-like roughness of the crystalline gadolinium layers, due to a columnar growth mechanism. This idea is further supported by the observation of increased intensity in the case of the X-ray diffraction spectra in figure 5 for a sample grown at an elevated substrate temperature, indicating a better degree of crystallinity within the layers rather than an increase in the rate of interdiffusion. The X-ray reflectivity spectra shown in figure 2 (d) then reveal a much larger degree of roughness present in the sample grown at elevated temperature, which can be related to a columnar-like growth mechanism [22].

The magnetic properties of U/Fe, U/Co and U/Gd multilayers are addressed in paper II of this series. Future measurements are planned to investigate the unusual growth mechanisms and structures of the U/Gd system, particularly the novel hcp U structure.

Acknowledgments

RS acknowledges the receipt of an EPSRC research studentship.

5. References

- [1] J A C Bland and B Heinrich. *Ultrathin Magnetic Structures*, volume 1. Springer, 1994.
- [2] L. Severin, L. Nordström, M. S. S. Brooks, and B. Johansson. *Phys. Rev. B*, 44:9392, 1991.
- [3] P. Fumagalli, T. S. Plaskett, D. Weller, T. R. McGuire, and R. J. Gambino. *Phy. Rev. Lett.*, 70:230, 1993.
- [4] N. Kernavanois, D. Mannix, P. Dalmas de Réotier, J. P. Sanchez, A. Yaouanc, A. Rogalev, G. H. Lander, and W. G. Stirling. *Phys. Rev. B*, 69:54405, 2004.
- [5] P. Fumagalli, T. S. Plaskett, T. R. McGuire, R. J. Gambino, and N. Bojarczuk. *Phy. Rev. B*, 46:6187, 1992.
- [6] M. A. Rosa, M. Diego, E. Alves, N. P. Barradas, M. Godinho, M. Almeida, and A. P. Gonçalves. *phys. stat. sol. (a)*, 196:153, 2003.
- [7] A M Beesley, M F Thomas, A D F Herring, R C C Ward, M R Wells, S Langridge, S D Brown, S W Zochowski, L Bouchenoire, W G Stirling, and G H Lander. *J. Phys.: Condens. Matter*, 16:8491, 2004.
- [8] A M Beesley, S W Zochowski, M F Thomas, A D F Herring, S Langridge, S D Brown, R C C Ward, M R Wells, R Springell, W G Stirling, and G H Lander. *J. Phys.: Condens. Matter*, 16:8507, 2004.
- [9] F. Wilhelm, N. Jaouen, A. Rogalev, W. G. Stirling, R. Springell, S. Zochowski, A. M. Beesley, S. D. Brown, M. F. Thomas, G. H. Lander, S. Langridge, R. C. C. Ward, and M. R. Wells. *Phys. Rev. B*, in press, 2007.
- [10] S. D. Brown, A. Beesley, A. Herring, D. Mannix, M. F. Thomas, P. Thompson, L. Bouchenoire, S. Langridge, G. H. Lander, W. G. Stirling, A. Mirone, R. C. C. Ward, M. R. Wells, and S. W. Zochowski. *J. Appl. Phys.*, 93:6519, 2003.
- [11] O. Hellwig, G. Song, H. W. Becker, A. Birkner, and H. Zabel. *Mat.-wiss. u. Werkstofftech.*, 31:856, 2000.
- [12] L. G. Parratt. *Phys. Rev.*, 95:359, 1954.
- [13] L. Nénot and P. Croce. *Revue Phys. Appl.*, 15:761, 1980.
- [14] S. K. Sinha, E. B. Sirota, S. Garoff, and H. B. Stanley. *Phys. Rev. B*, 38:2297, 1988.
- [15] K. Stoev and K. Sakurai. *The Rigaku Journal*, 14:22, 1997.
- [16] L. Nénot and P. Croce. *J. Appl. Cryst.*, 8:304, 1975.
- [17] S. Langridge. <http://www.rl.ac.uk/largescale/>.
- [18] R Springell, S W Zochowski, R C C Ward, M R Wells, S D Brown, L Bouchenoire, F Wilhelm, S Langridge, W G Stirling, and G H Lander.
- [19] A. L. Patterson. *Phys. Rev.*, 56:978, 1939.
- [20] L. Berbil-Bautista, Torben Hänke, Matthias Getzlaff, Roland Wiesendanger, Ingo Opahle, Klaus Koepnik, and Manuel Richter. *Phys. Rev. B*, 70:113401, 2004.
- [21] S. L. Molodtsov, J. Boysen, M. Richter, P. Segovia, C. Laubschat, S. A. Gorovikov, A. M. Ionov, G. V. Prudnikova, and V. K. Adamchuk. *Phys. Rev. B*, 57:13241, 1998.
- [22] J. A. Thornton. *J. Vac. Sci. Technol.*, 15:171, 1978.